JOURNAL OF THERMOPHYSICS AND HEAT TRANSFER
Vol. 13, No. 3, July–September 1999

Mathematical Modeling of Loop Heat Pipes and Experimental Validation

Tarik Kaya*
NASA Goddard Space Flight Center, Greenbelt, Maryland 20771
and
Triem T. Hoang†
TTH Research, Inc., Clifton, Virginia 20124

A mathematical model to calculate the steady-state performance of a loop heat pipe (LHP) is presented. The mathematical model is based on the steady-state energy conservation equations and the pressure drop calculations along the fluid path in the LHP. The LHP operating temperature is calculated as a function of the applied power at a given LHP condition. The heat exchange between each component of the LHP and the surroundings is taken into account. Both convection and radiation environments are modeled. Experimental validation of the model is attempted by using two different LHP designs. The validity of the mathematical model is investigated for different sink temperatures and elevations. The comparison of the calculations and experimental results showed good agreement (within 5%). The proposed method proved to be a useful tool for reliable prediction of the steady-state performance characteristics of the LHP.

Nomenclature

a_R = radiator area per length, m
C_P = specific heat at constant pressure, J/(kg-K)
D_{WICK} = diameter of wick, m
k_{EFF} = effective thermal conductivity of wick, W/(m-K)
k_L = liquid thermal conductivity of working fluid, W/(m-K)
k_{WICK} = thermal conductivity of wick material, W/(m-K)
L_C = length of condenser tube, m
L_{CC} = length of compensation chamber, m
L_{WICK} = length of wick, m
$\dot{m}$ = mass flow rate, kg/s
Nu_D = Nusselt number
P_{SAT} = saturation pressure, Pa
$\dot{Q}_{\mathrm{APP}}$ = total heat load applied to evaporator, W
$\dot{Q}_C$ = heat rejected by two-phase portion of condenser, W
$\dot{Q}_{\mathrm{CC-A}}$ = heat loss/gain between compensation chamber and ambient, W
$\dot{Q}_{\mathrm{HL}}$ = heat leak or back conduction, W
$\dot{Q}_{\mathrm{SC}}$ = heat required to bring returning subcooled liquid to saturation, W
$\dot{Q}_{\mathrm{VL-A}}$ = heat loss/gain between vapor line and ambient, W
T_{AMB} = ambient temperature, K
$T_R^{2\chi}$ = radiator temperature in two-phase portion of condenser, K
T_{SAT} = saturation temperature of loop heat pipe (LHP), K
T_{SINK} = sink temperature, K
TL = liquid line temperature, K
$(UA/L)_{\mathrm{C-A}}$ = thermal conductance per unit length from inner surface of condenser tube to ambient, W/(m-K)
$(UA/L)_{\mathrm{C-S}}$ = thermal conductance per unit length from inner surface of condenser tube to outer surface of condenser plate, W/(m-K)
$(UA/L)_{\mathrm{CC-A}}$ = thermal conductance per unit length from surface of compensation chamber to ambient, W/(m-K)
x = thermodynamic quality
z = axial coordinate, m
$\Delta T_{\mathrm{AC.WICK}}$ = temperature difference across wick, K
$\Delta P_{\mathrm{TOTAL}}$ = total presssure drop in LHP, Pa
ε = wick porosity and emissivity of radiator surface
η_R = radiator overall surface efficiency
λ = latent heat, W

Superscripts

L = liquid-filled portion of condenser
2χ = two-phase portion of condenser

Received 20 November 1998; presented as Paper 99-0477 at the 37th Aerospace Sciences Meeting, Reno, NV, 11–14 January 1999; revision received 22 February 1999; accepted for publication 23 February 1999.

*Resident Research Associate, National Research Council. Member AIAA.
†Senior Engineer.

I. Introduction

LOOP heat pipes (LHPs) are robust, self-starting, and passive two-phase thermal transport devices. The LHPs are used to transport excess heat from a heat source, such as payload instruments in a spacecraft, to a low-temperature heat sink, while maintaining the temperature within specified limits. An LHP uses the latent heat of vaporization of a working fluid to transfer heat and the surface tension forces formed in a fine-pore wick to circulate the working fluid. As shown in Fig. 1, a typical LHP consists of an evaporator, a reservoir (also called the compensation chamber or hydroaccumulator), vapor and liquid transport lines, a subcooler, and a condenser. The compensation chamber is thermally and hydrodynamically connected to the evaporator. In addition to the primary wick inside the evaporator, in many LHPs a secondary wick between the compensation chamber and the evaporator is also used to ensure that liquid remains available to the wick at all times.

During a typical LHP operation, after the heat is applied to the evaporator both the evaporator and the compensation chamber temperatures rise together, indicating back conduction or heat leak from the evaporator to the compensation chamber. The amount of the heat leak depends on the two-phase fluid dynamics between the evaporator and the compensation chamber. When the temperature difference between the evaporator and the compensation chamber is high enough to provide the required pressure difference to initiate

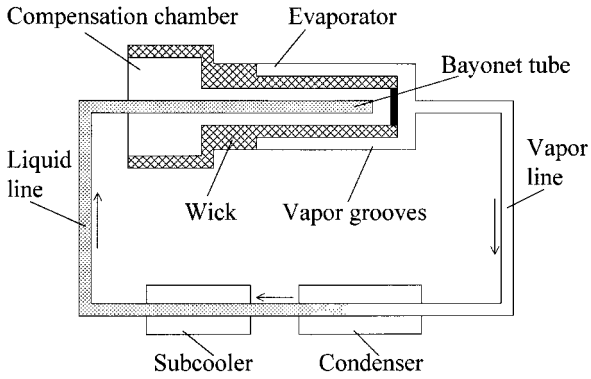

Fig. 1 Schematic of an LHP (not to scale).

the circulation of the fluid, the LHP starts. The start-up is identified by a sudden drop of the evaporator temperature and a sudden increase of the vapor line temperature. The vapor is collected in the vapor grooves and pushed into the vapor transport line because of the increased pressure from boiling. The meniscus inside the wick naturally adjusts itself to establish a capillary head that matches the total pressure drop in the LHP. The capillary head prevents vapor from penetrating into the wick structure. The vapor is then condensed in the condenser and later subcooled. The subcooler can be an integral part of the condenser. The subcooled liquid returns to the evaporator through the compensation chamber. A detailed thermodynamic analysis of a similar operation can be found in Ku.[1]

LHP can transport large thermal power loads, as much as 1.7 kW, over long distances through flexible and small diameter tubes and a heat flux of 0.70 MW/m^2 through the LHP evaporator was demonstrated.[2] Start-ups with as low as 2 W were achieved.[3] The LHP can also provide important heat rejection capability when they are positioned against gravity with an adverse elevation of the evaporator. 1.2 kW against a 4-m adverse elevation was demonstrated. Several ground applications are therefore feasible. The ability of the LHP to operate against gravity also makes ground testing of space applications possible. This is a clear advantage because of the high cost and limited availability associated with the space flight test programs. It is also possible to implement innovative technologies such as deployable radiators because of the flexible sections that can easily be incorporated into the LHP transport lines.[4]

The LHP is closely related to the capillary pumped loop (CPL). The CPL requires preconditioning prior to start-up and is more susceptible to deprime or loss of pumping action in the evaporator. However, the LHP can be started by directly applying heat to the evaporator and is largely resistant to the depriming problems caused by the presence of the bubbles in the evaporator core. Both technologies, however, exhibit extensive design flexibility to accommodate a large variety of thermal control requirements.[5] Hoang et al.[6] proposed a device that exhibits both CPL and LHP characteristics. This device has two conjoint independently operated loops: The main loop is basically a traditional CPL, and the auxiliary loop is similar to an LHP.

Altogether, these characteristics make the LHP very attractive thermal control devices in both ground and space applications. The LHP is currently the baseline design of the thermal control systems for NASA's Geoscience Laser Altimeter System (GLAS). The prediction is made that the use of the LHP as the primary thermal control system in space applications will rapidly increase in the near future. Because of their superior performance under high-g conditions, applications in aeronautical industry are under development. Specific applications include an avionics cooling[7] and anti-icing system for the engine cowl using waste engine heat.[8] The ground applications include rooftop solar installations and the cooling of remote communication sheds in a hot desert environment by transporting the heat into the ground and the cooling of semiconductor chips and reactors.

LHP was invented in the former Soviet Union in the early 1970s. The first patent was issued to Maidanik et al.[9] in 1985. In spite of the extensive ground testing of the LHP, only a limited number of flight tests was performed. The first flight test was conducted aboard a Russian spacecraft Granat in 1989 (Ref. 10). During this flight test, the long-term and reliable flight operation of LHP in microgravity was successfully demonstrated. Two successful flight experiments of American Loop Heat Pipe (ALPHA) proved over 56 hours of perfect on-orbit operation on the STS-83 and STS-94 missions in April and July 1997 (Ref. 4), respectively. Another successful flight test was performed on the STS-87 mission in November 1997 (Ref. 11). A total of 213 operating hours was accumulated during the mission. Summaries of the earlier experimental studies on the LHP can be found in two different articles analyzing the LHP performance characteristics by Dickey and Peterson[12] and Wirsch and Thomas.[13]

Because of the complexity of the related two-phase heat transfer phenomena, the LHP modeling efforts have mainly been focused on the steady-state energy balance equations. Many of the previous studies have either used oversimplified assumptions, or analyzed only one component of LHP. For some studies, the main algorithm of the model and the comparisons of numerical and experimental results were not revealed. Because of the commercial importance and relative recentness of this technology, only a limited amount of data and information has been published in the open literature.

Maidanik et al.[14] developed an analytical model with a closed-form solution by using the energy and pressure balances. They had to ignore heat exchange with ambient and pressure losses in the liquid line and assume a linear pressure drop in the vapor line to arrive at a closed analytical solution. Their heat-leak model is similar to the approach used in this study. Kiseev et al.[15] used a similar analytical model in their investigation focusing on increasing the heat transfer capacity of the LHP. Dickey and Peterson[12] developed an analytical model based on the steady-state energy balance equations with a different approach. Their model showed good agreement with the experimental data obtained at various tilts. In their work they limited the input power to less than 170 W. Bienert and Wolf[16] correlated successfully the LHP test data by using an analytical model based on the steady-state energy balance equations with a similar approach to the model presented in this article. However, in this study they did not discuss their model in sufficient detail. Wirsch and Thomas[13] focused mainly on the modeling of the evaporator section by using a two-dimensional finite element method. They validated their model experimentally for vapor line temperatures of 313 and 323 K. Several manufacturers have developed LHP models by using the SINDA/FLUINT solver, again based on energy balance equations. Lashley et al.[4] and Nikitkin and Cullimore[5] briefly referred to these models in their articles. Mulholland et al.[17] used an LHP model based on the study of Bienert and Wolf.[16] The liquid line of the LHP used in this study enters the transition section between the evaporator and the compensation chamber instead of the compensation chamber itself. Mulholland et al.,[17] therefore, introduced a weighting factor to modify the fluid temperature entering the wick. They also modified the code to account for condensers with parallel legs. Their model predictions showed good agreement with experimental results for power levels from 50 to 600 W and for condenser temperatures from 233 to 293 K.

More articles have been published on the modeling of the CPL performance in the open literature. However, these studies are not summarized here because of different working principles and therefore different modeling approaches between the LHP and CPL.

The present study complements the earlier modeling efforts of the LHP performance. The mathematical model was based on the steady-state energy conservation equations written for each component of the LHP. The temperature profile around the LHP was calculated with the help of these energy conservation equations and the pressure-drop calculations along the flowpath in the LHP. The heat exchange between each LHP component and the surroundings was modeled in both convection and radiation environments to validate experimental results in ambient and thermal vacuum conditions, respectively. The results of the model were compared with the experimental results, which were obtained by using two LHPs of different design. The experiments were conducted at different sink temperatures and at different elevations of the LHP. The comparison

between the model predictions and the experimental results showed good agreement, validating the mathematical model proposed in this study. The proposed model provides a design tool for a fast parametric study of the steady-state LHP performance. Special care was taken to explain the algorithm of the mathematical model in detail.

II. Mathematical Model

The LHP operating (saturation) temperature was calculated as a function of the input power at a given LHP condition. The specified LHP condition includes the sink temperature, the ambient temperature, and the elevation between the evaporator and the condenser. In this section the calculation algorithm for the convection environment will be presented in detail. The main difference in calculating the radiation environment will briefly be addressed at the end of this section.

The assumptions used in the development of the model are as follows:

1) The mass and heat transfer through the wick is only in the radial direction.

2) The compensation chamber and the evaporator core contain both liquid and vapor phases (two-phase fluid).

3) LHP achieves steady state for a given loop condition.

4) Single-phase flow correlations are employed to calculate the pressure drop in the condenser and subcooler.

The liquid-vapor interface can be in the vapor line, the condenser, the subcooler, or the liquid line, depending on the applied heat load and the sink temperature. The model can predict the operating temperature of the LHP for both cases: single-phase or two-phase fluid returning to the compensation chamber. If the charging strategy of the LHP is such that the compensation chamber is completely filled with liquid when the condenser is totally utilized, the model predictions will not be accurate because only two-phase fluid is allowed in the compensation chamber (assumption 2).

The relevant properties of the working fluid are saturation pressure, liquid density, vapor density, liquid viscosity, vapor viscosity, liquid thermal conductivity, liquid specific heat, and surface tension. These fluid properties are functions of the LHP operating temperature T_{SAT}. Each of these properties was curve fitted into a fifth-order polynomial with respect to T_{SAT} with errors of approximately 1–5%. The local liquid properties were calculated by using the average temperatures at each element of the LHP. The coefficients of the polynomials can be found in Ref. 18.

A. Solution Procedure

For a given applied heat load sink and ambient temperature and position of the LHP, the LHP operating temperature can be calculated by solving the energy balance equations of incoming and outgoing heat flows for each LHP component. To solve these equations, the relevant fluid properties, the system pressure drop, the mass flow rate, and the heat transfer coefficients should be known. However, these values are functions of the LHP operating temperature. Thus, the system of governing equations is an implicit function of the LHP operating temperature, and an iterative solution scheme is required.

The LHP saturation temperature is established in the compensation chamber as a result of three heat transfer paths: heat exchange between the evaporator and the compensation chamber (back conduction or heat leak), heat exchange between the compensation chamber and the environment, and heat exchange between the compensation chamber and the returning liquid. Active controlling of the LHP saturation temperature is thus possible by controlling the saturation temperature of the compensation chamber by a thermostatic heater. Under a steady-state operational condition the LHP operating temperature adjusts itself such that the condenser generates enough subcooling to match the heat leak and the heat exchange with the environment, which is given by the following equation:

$$\dot{Q}_{HL} = \dot{Q}_{SC} + \dot{Q}_{CC-A} \tag{1}$$

The axial conductive coupling between the evaporator and the compensation chamber was neglected in Eq. (1). This is a good approximation for an evaporator with high length-to-diameter ratio.

Heat Leak Across the Wick

The heat leak $\dot{Q}_{HL}$ from the high-pressure side of the wick to the low-pressure side is transferred through conduction, which can be written as

$$\dot{Q}_{HL} = \frac{2\pi k_{EFF} L_{WICK}}{\ell_n\left(D^{OUT}_{WICK} / D^{IN}_{WICK}\right)} \Delta T_{AC.WICK} \tag{2}$$

The heat exchange between the returning subcooled liquid and the wick material causes a nonlinear temperature profile. However, this is a small effect and can be neglected. The temperature difference across the wick $\Delta T_{AC.WICK}$ is the difference between the local saturation temperatures at both sides of the wick and caused by the total system pressure drop, excluding the pressure drop in the wick structure:

$$\Delta T_{AC.WICK} = \left(\frac{\partial T}{\partial P}\right)_{SAT} (\Delta P_{TOTAL} - \Delta P_{WICK}) \tag{3}$$

The slope of the vapor-pressure curve $(\partial T / \partial P)_{SAT}$ can be calculated using the Clausius–Clapeyron relation. However, because the fluid properties were curve fitted into the fifth-order polynomials with respect to T_{SAT}, the slope can be more accurately predicted if it is differentiated from the functional relationship between P_{SAT} and T_{SAT}.

Total System Pressure Drop of the LHP

The total system pressure drop ΔP_{TOTAL} in Eq. (3) is a function of the LHP operating temperature, the location of liquid-vapor interface in the condenser (which depends on the sink and ambient temperatures), and the amount of heat transported to the condenser. The total system pressure drop consists of the steady-state pressure drops in the vapor and liquid lines, the condenser, the subcooler, and the evaporator. The pressure drop in the evaporator includes those in the bayonet tube, the wick structure, and the vapor grooves. If the LHP is positioned with an elevation against gravity, the pressure difference caused by the gravitational forces should also be taken into account. Thus, the total system pressure drop is the sum of the pressure drops in individual components of the LHP along the flow path, i.e.,

$$\Delta P_{TOTAL} = \Delta P_{VL} + \Delta P_{LL} + \Delta P_C + \Delta P_{SC} + \Delta P_{BAY.TUBE} + \Delta P_{WICK} + \Delta P_{V.GRV} + \Delta P_{GRAVITY} \tag{4}$$

The pressure recovery caused by the deceleration of the fluid in the condenser and similarly the effect of the inertia terms in the vapor grooves were also taken into account. However, these effects are generally small, and the pressure drop in an LHP is largely dominated by the frictional pressure drops. When calculating the pressure drop in the evaporator, the effective length of the vapor grooves was taken as the half of the evaporator active length. The laminar and turbulent flow regimes were taken into account in these correlations. The calculation of the pressure drop constitutes an important part of the model because the temperature drop, and thus the heat leak from the evaporator to the compensation chamber, is directly related to the pressure drop. The model can predict the maximum heat transfer and vapor pressure limits. The prediction of the heat transfer limit was based on the fact that the sum of the pressure drops in the LHP cannot be greater than the maximum pressure created by the wick at the liquid-vapor interface for proper operation. The model can be extended to predict other operation limits; however, the capillary pressure limit is the dominant limiting factor for an ammonia LHP.

Effective Thermal Conductivity of the Wick

Two different correlations were used for the calculation of the effective thermal conductivity of the wick to analyze the influence of the different correlations on the results. A homogeneous and

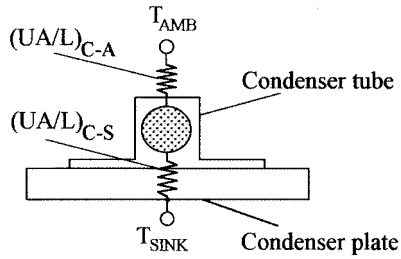

Fig. 2 Schematic of thermal resistance network of condenser.

isotropic wick structure was assumed. For the first correlation the effective thermal conductivity of the wick was obtained by volume averaging the thermal conductivity of the wick material and the working liquid inside the wick:

$$k_{\mathrm{EFF}} = k_{\mathrm{WICK}}(1-\varepsilon) + \varepsilon k_L \tag{5a}$$

For the second correlation the equation proposed by Dunn and Reay[19] was used:

$$k_{\mathrm{EFF}} = k_{\mathrm{WICK}}\left\{\frac{2+(k_L/k_{\mathrm{WICK}})-2\varepsilon[1-(k_L/k_{\mathrm{WICK}})]}{2+(k_L/k_{\mathrm{WICK}})+\varepsilon[1-(k_L/k_{\mathrm{WICK}})]}\right\} \tag{5b}$$

Heat Transfer Coefficients

The thermal conductances of the condenser and the subcooler were calculated by considering the thermal resistance network shown in Fig. 2. In the convection environment the heat exchange between the LHP and the ambient were assumed to be natural convection. The simplified natural convection correlations for air from Ref. 20 were used to calculate the heat transfer coefficients from the LHP element surfaces to ambient. The thermal conductance from the inner surface of the condenser tube to the external surface of the condenser plate was computed by considering the flow arrangement of the heat exchanger, including the heat conduction in the condenser plate. The convective film coefficient caused by the fluid flow inside the condenser tube was calculated as a function of the operating temperature.

As an example, the thermal conductance per unit length from the liquid-filled portion of the condenser tube to the sink was calculated by using the following thermal network:

$$\left(\frac{UA}{L}\right)^{L}_{\mathrm{C-S}} = \frac{1}{1/(UA/L)_{\mathrm{C-S}} + 1/(\pi Nu_D k_L)} \tag{6}$$

The first term in right side of Eq. (6) was determined by considering the thermal resistances for conduction from the appropriate geometric parameters of condenser and the flow arrangement. The thermal contact resistance between the condenser tube and the condenser plate should also be taken into account. For the second term the Nusselt number Nu_D is constant for a laminar and fully developed flow and equal to $Nu_D = 4.36$ if the surface heat flux is constant, and $Nu_D = 3.66$ if the surface temperature is constant.[21]

Returning Liquid Subcooling

The heat rejected in the two-phase portion of the condenser $\dot{Q}_C$ can be written as

$$\dot{Q}_C = \dot{Q}_{\mathrm{APP}} - \dot{Q}_{\mathrm{HL}} - \dot{Q}_{\mathrm{VL-A}} \tag{7}$$

The heat exchange between the vapor transport line and ambient can be positive or negative depending on the sink and ambient temperatures. The two-phase heat removal in the condenser tube consists of two parts: heat rejection to the sink and heat lost to ambient. Thus, the length of the two-phase flow portion in the condenser is given by

$$L_C^{2\chi} = \dot{Q}_C \times \int_{x_{\mathrm{IN}}}^{x_{\mathrm{OUT}}} \frac{\mathrm{d}x}{\left[(UA/L)^{2\chi}_{\mathrm{C-S}}(T_{\mathrm{SAT}}-T_{\mathrm{SINK}}) + (UA/L)^{2\chi}_{\mathrm{C-A}}(T_{\mathrm{SAT}}-T_{\mathrm{AMB}})\right]} \tag{8}$$

The related thermal conductances in the parentheses were calculated by considering the thermal resistance network of each heat transfer path, as explained in the preceding section. The thermal conductance in the two-phase portion of the condenser was calculated by using a two-phase multiplier. For a simple and reasonable approximation, the expression proposed by Chato[22] for the condensation heat transfer coefficient in horizontal tubes can also be used.

If the result of the integration of Eq. (8) with respect to the quality from $x_{\mathrm{IN}} = 1$ to $x_{\mathrm{OUT}} = 0$ is less than the total length of the condenser, the liquid-vapor interface is situated inside the condenser. Otherwise, the same calculation methodology can be used to compute the location of the liquid-vapor interface first in the subcooler, then in the liquid line. After the calculation of the length of the two-phase flow portion in the condenser, the liquid temperature at the condenser exit can be calculated by integrating the energy balance equation in the liquid-filled portion of the condenser, i.e.,

$$\frac{\dot{Q}_C}{\lambda}C_P\frac{\mathrm{d}T}{\mathrm{d}z} = \left(\frac{UA}{L}\right)^{L}_{\mathrm{C-S}}(T-T_{\mathrm{SINK}}) + \left(\frac{UA}{L}\right)^{L}_{\mathrm{C-A}}(T-T_{\mathrm{AMB}}) \tag{9}$$

where T represents the local fluid temperature.

If the LHP contains an additional subcooler unit, Eq. (9) can be applied to the subcooler unit to calculate the exit temperature. Similarly, the same equation is valid to calculate the liquid line exit temperature. The amount of heat required to bring the returning subcooled liquid to saturation is given by

$$\dot{Q}_{\mathrm{SC}} = \dot{m}C_p(T_{\mathrm{SAT}} - TL_{\mathrm{OUT}}) \tag{10}$$

LHP Operating Temperature

The heat loss or gain between the compensation chamber and ambient can be written as

$$\dot{Q}_{\mathrm{CC-A}} = (UA/L)_{\mathrm{CC-A}}L_{\mathrm{CC}}(T_{\mathrm{SAT}} - T_{\mathrm{AMB}}) \tag{11}$$

By substituting Eqs. (2), (10), and (11) into Eq. (1), one will obtain the following equation:

$$F_1(T_{\mathrm{SAT}}, T_{\mathrm{SINK}}, T_{\mathrm{AMB}}, \dot{Q}_{\mathrm{APP}}) = F_2(T_{\mathrm{SAT}}, T_{\mathrm{SINK}}, T_{\mathrm{AMB}}, \dot{Q}_{\mathrm{APP}}) + F_3(T_{\mathrm{SAT}}, T_{\mathrm{AMB}}) \tag{12}$$

where F_1, F_2, and F_3 are known functions. For given T_{SINK}, T_{AMB}, and $\dot{Q}_{\mathrm{APP}}$, the LHP operating temperature can be determined by solving Eq. (12) iteratively for T_{SAT}. The convergence was assumed to occur when $|F_1 - (F_2 + F_3)| < 10^{-3}$ W. To accelerate the convergence of the solutions, the operating temperature at each iteration was corrected as a function of the residual of Eq. (12) between the two successive iterations. A typical converged solution for a given heat load was reached at approximately 1000 iterations. It took approximately 5 s to reach a converged solution at a given power level by using a 120-MHz Pentium processor.

B. Radiation Environment

The general algorithm used to calculate the radiation environment is the same as that of the convection environment. When the liquid-vapor interface is in the condenser, the heat removal by radiation in the two-phase portion of the condenser can be written as follows:

$$\dot{Q}_C = (UA/L)^{2\chi}_{\mathrm{C-S}}L_C^{2\chi}\left(T_{\mathrm{SAT}} - T_R^{2\chi}\right) = \sigma\varepsilon\eta_R a_R L_C^{2\chi}\left[\left(T_R^{2\chi}\right)^4 - (T_{\mathrm{SINK}})^4\right] \tag{13}$$

The radiator temperature $T_R^{2\chi}$ and the length of the two-phase portion of the condenser $L_C^{2\chi}$ can be calculated by using Eq. (13). Similarly, the heat exchange equations between the LHP components and environment presented in the preceding section should be replaced by the radiation heat transfer equations. The calculation of the returning liquid subcooling follows the same method as that of the convection environment.

III. Experimental Setup

Two separate test programs were conducted at the NASA Goddard Space Flight Center to verify the mathematical model. In the first test program an LHP designed for the thermal control of the GLAS instrument was used. The second test program was performed on a research LHP designed for the U.S. Naval Research Laboratory (NRL). A complete discussion of the performance characteristics of each LHP can be found respectively in Refs. 23 and 24. In this section the instrumentation and test procedure will be explained with a brief description of each LHP.

A. Instrumentation and Test Procedure

To monitor the temperature profiles of the LHP and environment, more than 45 copper/constantan (type T) thermocouples were placed at various locations throughout each LHP. The uncertainty of the thermocouple readings was estimated to be ± 0.5 K. The heat source consisted of cartridge and tape heaters. Aluminum and copper saddles were welded to the evaporator to provide mounting surfaces for electrical heaters. Heaters were mounted either on only one side or on both sides of the evaporator saddles. Tape heaters were attached to the compensation chamber to control the set point temperature for some of the tests. Relays and variacs were used to control the heaters. The uncertainty in measuring the power input was estimated to be less than 2%.

The condenser lines were coupled to the cooling lines, which were cooled by refrigerators with a 1.5 kW cooling capacity. A mixture of ethlyene glycol (60%)/water (40%) was used as coolant fluid. The heat rejection system was able to maintain the sink temperature within ± 1 K of the chosen set point. Some high-frequency oscillations of the sink temperature were observed. However, the effect of these fluctuations on the system performance was negligible because the induced fluctuations in the working fluid temperatures caused by these fluctuations were less than ± 0.25 K. The LHP were insulated with 15 mm-thick Armaflex material.

All measurements were taken with a computerized data acquisition system. Data were displayed in real time and stored for later analysis. The sampling rate of data was 10 kHz with a resolution of 16-bit and an analog-to-digital system accuracy of 0.6%.

During a typical test, the first step was to set the condenser temperature at a desired value. Once the condenser reached the steady state, the power was applied to the evaporator. At each power level the system was allowed to reach a steady state. This would take more than 5 h at low powers (< 100 W) and approximately 0.5 h at high powers. Tests were performed by cycling the power and the sink temperature at various positive and adverse elevations.

B. Characteristics of the GLAS LHP

The GLAS LHP (LHP1) had a cylindrical evaporator with a diameter of 25.4 mm and a length of 150 mm. The evaporator's envelope was constructed of low-carbon steel, and it used a sintered nickel wick with an effective pore radius of less than 1.2 μ. The working fluid of the LHP was ammonia. A copper saddle was attached to the evaporator's envelope to hold three cartridge heaters. The compensation chamber had a diameter of 46 mm and a length of 76 mm. Both the liquid and vapor transport lines were approximately 460 mm long each. They were made from smooth wall tubing with a diameter of 5.54 mm and a wall thickness of 0.51 mm. The condenser was a single pass, direct condensation heat-exchanger type with a total length of 4.06 m and a condenser tube outer diameter of 5.54 mm and was made from an extruded small diameter aluminum tube with an integral fin. The condenser tube was bent into serpentine shape, which made passes across a condenser plate of 485×1000 mm. The refrigerated coolant flowed through another tube, which ran parallel to the condenser tube on the other side of the condenser plate. The thermal conductance per unit length from the inner surface of the condenser tube to the outer surface of the condenser plate was 4 W/(m-K).

C. Characteristics of NRL LHP

The NRL LHP (LHP2) had a cylindrical evaporator of 25.4 mm in diameter and 305 mm in length. The compensation chamber had the same diameter as the evaporator and was 127 mm long. A sintered nickel wick with an effective pore radius of less than 1.2 μ was used. The LHP used ammonia as its working fluid. The evaporator was embedded into an aluminum saddle so that heat could spread evenly on the upper side of evaporator. The liquid and vapor transport lines were made of 4.8-mm outer-diameter stainless-steel tubing and had an overall length of about 1524 mm each. The condenser consisted of three separate sections linked in series and was made up of 4.8-mm-outer diameter stainless-steel tubing with an overall length of 2032 mm. The condenser was similar to that of LHP1 (i.e., single pass and direct condensation heat exchanger). However, no condenser plate was employed. The condenser line was attached to the coolant loop by small aluminum saddles, and epoxy fillings were used between the condenser and coolant tubes to minimize the thermal contact resistance. The thermal conductance per unit length from the inner surface of the condenser tube to the outer surface of the condenser plate was 6 W/(m-K).

IV. Discussion of Results

Results were presented on the LHP performance curve (applied power vs operating temperature). Figure 3 shows the comparison between the experimental results and the predictions for LHP1. The experimental results were obtained at eight different power levels for two distinct sink temperatures of 273 and 283 K. The condenser plate was in vertical position such that the evaporator and the compensation chamber were leveled horizontally within ± 2.5 mm. In comparing the results, the difference between the model predictions and the experimental results was normalized by the sink temperature. The calculations are within 2% of the experimental measurements. As shown in Fig. 3, at lower powers (approximately less than 100 W) the operating temperature initially decreases with increasing power because of the cold liquid returning from the condenser. In this region the LHP is in the variable conductance mode. At a certain power the condenser becomes completely open, and the LHP operates in the constant conductance mode. At this point the operating temperature increases almost linearly with the applied power. The operating temperature predictions at low powers are less satisfactory (around 2%). The discrepancy is because of the effect of the heat exchange with ambient is more pronounced at low powers. More precise correlations than simplified natural convection equations are required to improve the results in this region. The operating temperature predictions at low powers were also less accurate in Bienert and Wolf[16] because of probably the same difficulty in modeling the heat exchange between the compensation chamber and ambient. At higher powers, the energy balance is dominated by the liquid returning from the condenser rather than the heat exchange with ambient. In fact, the heat exchange with ambient becomes a smaller fraction of the applied heat with increasing power (e.g., 1.2% at 25 W and 0.2% at 200 W). As a result, the predictions are better at high powers (within 1%).

As shown in Fig. 3, when the sink temperature is increased from 273 to 283 K the LHP performance curve shifts toward higher operating temperatures. The lowest operating temperature on the curve also shifts toward lower power levels because less subcooling is provided when the sink temperature gets closer to the ambient temperature. In fact, when the sink temperature is equal to ambient,

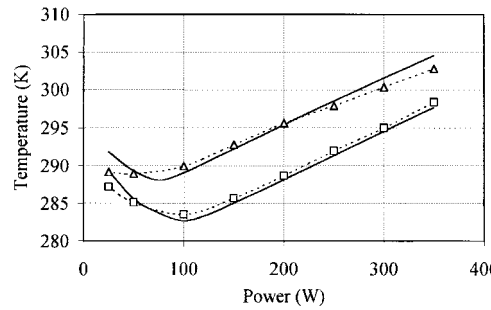

Fig. 3 Comparison of experimental results and model predictions for LHP1 at $T_{AMB} = 295$ K: □, measurements at $T_{SINK} = 273$ K; △, measurements at $T_{SINK} = 283$ K; and ——, predictions.

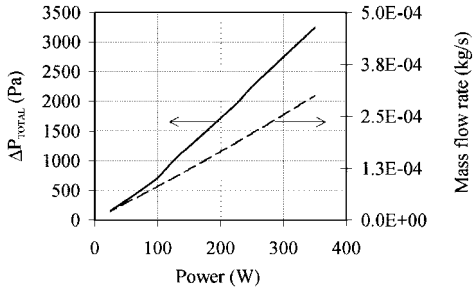

Fig. 4 Calculated total pressure drop and mass flow rate curves for LHP1 at T_{AMB} = 295 K and T_{SINK} = 283 K.

no subcooling is provided by the condenser, and the LHP operates entirely in the fixed conductance mode.

The corresponding calculated total pressure drop in the LHP and the mass flow rate as a function of the applied power is shown in Fig. 4 for a sink temperature of 283 K. Both the total pressure drop and the mass flow rate increase with increasing applied power. The sudden increase in the slope of the total pressure drop around 100 W is because of the transition from the laminar to the turbulent flow regime. Figure 4 also shows that the mass flow rate is very small at low powers. Therefore, little cooling is initially provided to the compensation chamber at low powers. As the heat load increases, although more and more condenser area becomes active, the amount of heat required to bring returning subcooled liquid to saturation increases because of the higher mass flow associated with the increasing heat input. As a result, the LHP operating temperature drops in the low power region with increasing power. If the heat load is further increased until the condenser is completely open, the temperature of the returning liquid is near saturation, and initially no subcooling is available. At some power level the saturation temperature starts increasing with increasing heat load to allow the condenser to reject additional heat. This explanation is consistent with the earlier statement in the preceding paragraph for the operation under the equal sink and ambient temperatures. Two different correlations for the wick effective thermal conductivity [Eqs. (5a) and (5b)] were used to study the influence of these correlations on the results. The difference in the operating temperatures was less than 0.03%, suggesting that either of these two correlations can be used within the operation limits of interest.

The frictional pressure drop in the condensing zone of the condenser was calculated using a correlation based on the single-phase flow (all vapor). However, the pressure drop in the condenser was reasonably well predicted because the pressure drop in the condenser was less than 20% of the total pressure drop for the operating conditions studied in this work. The results obtained by using a two-phase flow pressure drop model will be presented in a future paper.

Because of the maximum power limit of the heaters used in this study, the heat transport limit predictions could not be verified experimentally. However, the observation was made experimentally that at high powers the primary wick may experience partial dry-out because of the several factors such as uneven heating before the maximum heat transfer capacity was reached. This mode of operation is different from that of a CPL. In a CPL, after vapor penetrates the wick it blocks the liquid flow, hence depriming the evaporator. Whereas in a LHP, because of the secondary wick a part of the primary wick is always wet, and the LHP can still operate. After the partial dry-out the LHP performance characteristics are drastically modified. The present model cannot predict the LHP performance if partial dry-out of the wick occurs.

Figure 5 shows the result obtained by using LHP2. The experimental results were obtained by using five different power profiles (from A to E). The power profiles for each cycle are given in Table 1. Each of the power cycles from A to D took approximately 10 h to complete, and the power cycle E took approximately 72 h. This was because of the long waiting times, especially at low powers (less than 100 W) to reach the steady-state operation. The ambient temperature change during these tests was approximately 2.0 K, and an

Table 1 Power profiles for different test cycles

Cycle	Power profile, W
A	50-5-50
B	2-10-25-50-100
C	5-10-25-50-100-50-25
D	5-10-25-50-100-200-300-400-300-200-100-200
E	10-25-50-100-200-300-400-300-200-100-50-400-50-100-200-300-400-100-700-100-50-100-200-100-700-600-500-400-300-200-100-50

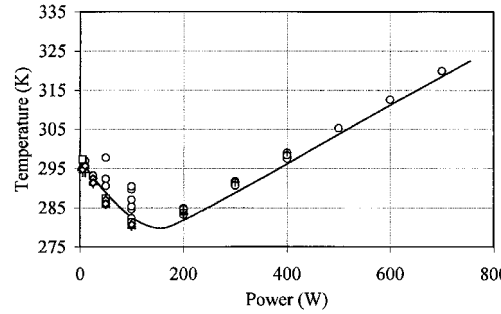

Fig. 5 Comparison of experimental results and model predictions for LHP2 at T_{AMB} = 294 K, T_{SINK} = 263 K, and no elevation: □, cycle (A); △, cycle (B); ◇, cycle (C); +, cycle (D); ○, cycle (E); and ——, predictions.

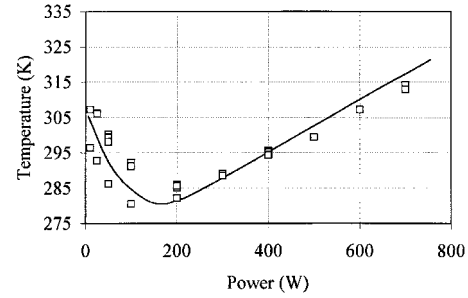

Fig. 6 Comparison of experimental results and model predictions for LHP2 at T_{AMB} = 294 K, T_{SINK} = 263 K, and an elevation of 660 mm: □, measurements; and ——, predictions.

average ambient temperature was used in the calculations for each cycle. All of the tests were conducted with a sink temperature of 263 K, and the LHP was leveled horizontally within ±2.5 mm such that the evaporator, the compensation chamber, and the condenser were in the same horizontal plane.

During the power-cycling tests, a temperature hysteresis was observed at power levels less than 200 W. This phenomenon was discussed in detail in Ref. 24. When the power was decreased with a moderate step change (less than 100 W), the operating temperatures values were stable. However, when the power was decreased with a larger step, the LHP operating temperatures were deviated from their initial steady-state values in the low-power region. The temperature hysteresis phenomenon in a LHP is still unexplained. The scattered points at low powers presented in Fig. 5 are because of this temperature hysteresis phenomenon. The model predictions are between 1.5–5% of the experimental measurements. At high powers the temperatures were highly stable regardless of the power-cycling profile, and the model predictions were very satisfactory. The mathematical model used in this study cannot predict the temperature hysteresis.

The mathematical model was also tested when the LHP was positioned at an elevation with the evaporator and the compensation chamber leveled horizontally above the condenser. A typical comparison is presented in Fig. 6 for an elevation of 660 mm (vertical distance between the evaporator axis and the lowest point of the LHP). The experimental results were obtained by using the power cycle E given in Table 1. The temperature hysteresis is clear at low powers, and model predictions are within 5%. As shown in Fig. 6,

the model predicted only the overall tendency of the LHP performance curve at low powers. The comparison of the experimental results and the calculations are again more satisfactory at high powers (within 2.5%).

V. Conclusions

The LHP research is an important and current field of study because of the great potential use of this device. In this study a mathematical model to calculate the steady-state performance of an LHP was presented in detail. The mathematical model was tested with two separate LHP designs at different sink temperatures and different elevations. The calculations were between 1 and 5% of the experimental measurements, indicating that the steady-state LHP performance was accurately modeled. The predictions were less satisfactory at low-power regions (less than approximately 100 W), where the heat exchange with ambient has a bigger influence on the energy balance of the compensation chamber. Agreement could be improved by using more precise correlations for the natural convection heat transfer coefficients. The pressure-drop predictions in the condenser section can be improved by using two-phase flow correlations. An important observation at low powers was the temperature hysteresis. The model cannot predict the temperature hysteresis; however, the calculations appear to be in good accord with the experimental results. As a result, the model can be used for a reasonable assessment of the overall LHP performance even in the presence of the temperature hysteresis.

The temperature hysteresis has not been well understood and has not been adequately addressed in open literature. A better understanding of the physical mechanism behind the temperature hysteresis is required for its modeling. Further tests in thermal vacuum environment are also required to validate the radiation heat transfer part of the mathematical model. Because the start-up and related transients constitute a very important problem of the two-phase flow devices, the consideration of the unsteady effects is also needed to improve this mathematical model.

Acknowledgments

This work was performed at NASA Goddard Space Flight Center (GSFC). One of the test articles was on loan from the U.S. Naval Research Laboratory (NRL). The help of Jentung Ku of NASA GSFC and Kwok Cheung of NRL is greatly appreciated. Part of the funding for this work was provided by National Research Council–NASA GSFC Research Associateship Grant.

References

[1]Ku, J., "Thermodynamic Aspects of Capillary Pumped Loop Operation," AIAA Paper 94-2059, June 1994.

[2]North, M., Sarraf, D., Rosenfeld, J., Maidanik, Y., and Vershinin, S., "High Heat Flux Loop Heat Pipes," *American Institute of Physics Conference Proceedings 970115*, edited by M. S. El-Genk, American Inst. of Physics, New York, 1997, pp. 561–566.

[3]Kaya, T., Ku, J., Hoang, T. T., and Cheung, M. K., "Investigation of Low Power Start-Up Characteristics of a Loop Heat Pipe," *American Institute of Physics Conference Proceedings 458*, edited by M. S. El-Genk, American Inst. of Physics, New York, 1999, pp. 799–804.

[4]Lashley, C., Krein, S., and Barcomb, P., "Deployable Radiators—A Multi-Discipline Approach," Society of Automotive Engineers, Paper 981691, July 1998.

[5]Nikitkin, M., and Cullimore, B., "CPL and LHP Technologies: What Are the Differences, What Are the Similarities?" Society of Automotive Engineers, Paper 981587, July 1998.

[6]Hoang, T. T., Cheung, K. M., and Kim, J. H. "Design and Test of a Proof-of-Concept Advanced Capillary Pumped Loop," Society of Automotive Engineers, Paper 972326, July 1997.

[7]Gernert, N. J., Baldassarre, G. J., and Gottschlich, J. M., "Loop Heat Pipes for Avionics Thermal Control," Society of Automotive Engineers, Paper 961318, July 1996.

[8]Phillips, A. L., and Gernert, N. J., "Loop Heat Pipe Anti-Icing System for UAV," Intersociety Engineering Conf. Energy Conversion, Paper 98-240, Colorado Springs, CO, Aug. 1998.

[9]Maidanik, Y. F., Vershinin, S., Kholodov, V., and Dolggirev, J., "Heat Transfer Apparatus," U.S. Patent 4515209, May 1985.

[10]Maidanik, Y. F., Fershtater, Y. G., and Goncharov, K. A., "Capillary Pumped Loop for the Systems of Thermal Regulation of Spacecraft," *Proceedings of the 4th European Symposium on Space Environmental and Control Systems*, ESA SP-324, 1991.

[11]Bienert, W. B., "Loop Heat Pipe Flight Experiment," *American Institute of Physics Conference Proceedings 420*, edited by M. S. El-Genk, American Inst. of Physics, New York, 1998, pp. 511–513.

[12]Dickey, J. T., and Peterson, G. P., "An Experimental and Analytical Investigation of the Operational Characteristics of a Capillary Pumped Loop," *Journal of Thermophysics and Heat Transfer*, Vol. 8, No. 3, 1994, pp. 602–607.

[13]Wirsch, P. J., and Thomas, S. K., "Performance Characteristics of a Stainless Steel/Ammonia Loop Heat Pipe," *Journal of Thermophysics and Heat Transfer*, Vol. 10, No. 3, 1996, pp. 326–333.

[14]Maidanik, Y. F., Fershtater, Y. F., and Solodovnik, N. N., "Design and Investigation of Regulation of Loop Heat Pipes for Terrestrial and Space Applications," Society of Automotive Engineers, Paper 941407, June 1994.

[15]Kiseev, V. M., Belonogov, A. G., and Pogorelov, N. P., "Development of Two-Phase Loops with Capillary Pumps," Society of Automotive Engineers, Paper 972482, July 1997.

[16]Bienert, W. B., and Wolf, D. A., "Temperature Control with Loop Heat Pipes: Analytical Model and Test Results," *Proceedings of the 9th International Heat Pipe Conference*, Los Alamos National Lab., Los Alamos, NM, 1995.

[17]Mulholland, G., Gerhart, C., Gluck, D., and Stanley, S., "Comparison Between Analytical Predictions and Experimental Data for a Loop Heat Pipe," *American Institute of Physics Conference Proceedings 458*, edited by M. S. El-Genk, American Inst. of Physics, New York, 1999, pp. 805–810.

[18]Brennan, P. J., and Kroliczek, E. J., "Heat Pipe Design Handbook," NASA Contract NAS5-32406, Vol. 2, June 1979, pp. 62–67.

[19]Dunn, P. D., and Reay, D. A., *Heat Pipes*, Pergamon, Oxford, 1994, p. 122.

[20]Holman, J. P., *Heat Transfer*, 4th ed., McGraw–Hill, New York, 1977, p. 253.

[21]Incropera, F. P., and De Witt D. P., *Fundamentals of Heat and Mass Transfer*, 3rd ed., Wiley, New York, 1990, p. 491.

[22]Chato, J. C., "Laminar Condensation Inside Horizontal and Inclined Tubes," *Journal of American Society of Heating, Refrigerating and Air Conditioning Engineers*, Vol. 4, No. 52, 1962, pp. 52–60.

[23]Douglas, D., Ku, J., and Kaya, T., "Testing of the Geoscience Laser Altimeter System Prototype Loop Heat Pipe," AIAA Paper 99-0473, Jan. 1999.

[24]Cheung, M. K., Hoang, T. T., Ku, J., and Kaya, T., "Thermal Performance and Operational Characteristics of Loop Heat Pipe (NRL LHP)," Society of Automotive Engineers, Paper 981813, July 1998.